Creating FDTD models of commercial GPR antennas using Taguchi's optimisation method

Craig Warren* and Antonios Giannopoulos**

ABSTRACT

Very few researchers have developed numerical models of Ground-Penetrating Radar (GPR) that include realistic descriptions of both the antennas and the subsurface. This is essential to be able to accurately predict responses from near-surface, near-field targets. This paper presents detailed three-dimensional (3D) Finite-Difference Time-Domain (FDTD) models of two commercial GPR antennas—a Geophysical Survey Systems, Inc. (GSSI) 1.5 GHz antenna and a MALÅ Geoscience 1.2 GHz antenna—developed using simple analyses of the geometries and the main components of the antennas. Values for unknown parameters in the antenna models (due to commercial sensitivity) were estimated by using Taguchi's optimisation method, resulting in a good match between the real and modelled crosstalk responses in free-space. Validation using a series of oil-in-water emulsions to simulate the electrical properties of real materials demonstrated that it was essential to accurately model the permittivity and dispersive conductivity. When accurate descriptions of the emulsions were combined with the antenna models the simulated responses showed very good agreement with real data. This provides confidence for use of the antenna models in more advanced studies.

INTRODUCTION

Ground-Penetrating Radar (GPR) is a non-destructive, electromagnetic, investigative tool used mainly in the fields of geophysics and engineering. The numerical modelling of GPR has been an active area of research since the early 1990's, and the sophistication, size, and dimensionality of GPR models have accelerated rapidly over the years as computational resources have improved and become more accessible. One of the key drivers for accurate forward models of GPR is the knowledge that the interpretation of GPR data is application-specific, and highly dependent on the skill and experience of the user. Thus, an accurate GPR forward model is an extremely useful tool for furthering knowledge in many areas of GPR research.

A typical GPR survey includes the GPR system, the subsurface or structure, and any potential targets. All of these components must be included in a forward model, if real responses are to be directly compared with modelled data. Despite many models including realistic descriptions of the subsurface most replace the GPR system with a theoretical source such as an infinitesimal dipole. This type of source model is suitable for investigating targets in the far-field of the antenna e.g. if the antenna is raised off the ground, or if the targets are deeply buried. However typically the antenna is ground-coupled and targets are near the surface, therefore in the near-field of the antenna. This means the direct wave from the antenna, and the response from the target can overlap. To accurately model the phase and amplitude information in this type of response the actual transmitter and receiver antennas must be included in the simulation.

Most previous research where either realistic descriptions of the subsurface or the GPR antennas have been included in simulations can be grouped into two areas:

- Antenna design: improvement of the classic bowtie design or investigation of new antenna designs for GPR.
- Development of models with realistic subsurface properties.

Some studies overlap both these areas but few have directly compared modelled and measured amplitude and phase information, and none have done so with widely-used commercial GPR antennas.

In the area of antenna design several researchers have numerically modelled, and studied the performance and characteristics of their own custom-built GPR antennas (van Coevorden et al., 2006; Huang et al., 1999; Lestari

et al., 2004, 2005; Monorchio et al., 2004; Shlager et al., 1994; Uduwawala and Norgren, 2006). Their antennas were planar or wire bowties, and loaded by discrete resistors or electromagnetic absorber material. All the models were 3D and most utilised the Finite-Difference Time-Domain (FDTD) method. The structure and geometry of the antennas were always included in the models, as well as either the loading resistors or absorber material. Both Shlager et al. (1994) and Lestari et al. (2004, 2005) verified the results of their simulations against experimental data with good agreement.

Bourgeois and Smith (1996) were the first to include a realistic description of GPR antennas over a subsurface in their 3D FDTD model that replicated an experimental scale-model of a GPR system. However, it was acknowledged that because the model domain was truncated using Perfect Electric Conductor (PEC) boundaries, there were unwanted reflections in the modelled responses that were difficult to remove. Roberts and Daniels (1997) created 3D models of 300 MHz unshielded bowties and compared the modelled radiation patterns with measured data (Wensink et al., 1990), as well as comparing scattering responses from metallic and plastic pipes submerged in the water (Wensink et al., 1991). Roberts and Daniels (1997) notably mentioned a lack of comparison of real and modelled amplitude data. Their best agreement reached between modelled and measured data over buried targets had a peak difference of 3.3 dB.

More recent studies that have included realistic models of the subsurface have either used an infinitesimal dipole source model or have been a custom antenna design (Holliger et al., 2003; Liu et al., 2008; Nishioka et al., 1999; Uduwawala et al., 2004, 2005). Lambot et al. (2004) used a system of linear transfer functions to model a GPR system which used a step-frequency continuous-wave (SFCW) radar combined with a monostatic transverse electromagetic (TEM) horn antenna designed to be used off-ground. A point source model was used as the targets were in the far-field of the antenna. Very good agreement was shown for both phase and amplitude information of the modelled and measured responses in layered soil. Oden (2006) created a 3D FDTD model of a 50 MHz antenna containing absorber material. Time-domain reflectometry was used to measure the response of the transmitting and receiving circuitry. The modelled system response compared favourably with measurements from the real system made in air and over water.

Klysz et al. (2006) presented one of the first attempts at modelling a widely-used commercial GPR antenna. Results from a 3D FDTD model of a GSSI 1.5 GHz antenna showed some similarity with measured free-space radiation patterns, but significantly the model did not include the receiver antenna. Streich and van der Kruk (2007) characterised a MALÅ 100 MHz antenna in free-space by inverting electric field measurements. Small differences were observed between the measured electric field data and those simulated from the best-fit inversion model. Lambot et al. (2010) extended previous work (Lambot et al., 2004) to model, using transfer functions, the near field of a GSSI 900 MHz using a series of point sources and receivers.

In this paper, detailed models of two commercial GPR antennas are developed from simple analyses of the geometries and main components of the antennas. In the first part of the paper analyses of the geometries, components and materials of the antennas are presented. Then 3D FDTD models of the antennas are developed, utilising Taguchi's optimisation process to determine values of unknown parameters in the antennas. Finally, the antenna models are validated by comparing responses from a series of experiments in which typical GPR targets are embedded in emulsions, to simulations of the experiments which include the antenna models.

DEVELOPMENT OF THE MODELS

Computational tools

The electromagnetic simulation software is an essential element of any GPR forward model. All of the simulations in this research used GprMax3D which is part of GprMax, a suite of electromagnetic wave simulators based on the FDTD method. GprMax (http://www.gprmax.org/) is freely available software that was written by Giannopoulos (2005) originally in 1996, and has since developed into a mature application that has been successfully used by a number of researchers (Galagedara et al., 2005; Jeannin et al., 2006; Lopera and Milisavljevic, 2007; Soldovieri et al., 2007). GprMax computes the spatial and temporal derivatives using a standard second-order scheme. Higher order FDTD schemes have longer computational stencils when compared with the standard second-order scheme. As a result the efficient handling of boundaries in a model can be problematic, especially for metallic objects. In the case of a pure dielectric model where some fuzziness on the location of boundaries is acceptable, a higher order scheme could be beneficial. However, this is not the case in this work as fine details need to be included in the antenna models. GprMax contains a number of features important for modelling GPR antennas:

- Perfectly Matched Layer (PML) (Berenger, 1994) boundaries based on the Uniaxial Perfectly Matched Layer (UPML) (Gedney, 1996) allowing the computational domain to be effectively truncated. This is especially important for modelling antennas because models can be computationally expensive and thus a minimal, effective PML is extremely beneficial.
- User specified excitation functions allowing custom pulse shapes with specific frequency content to be used for source excitation.
- Voltage source and transmission line feed models.
- Code parallisation using OpenMP (http://openmp.org/) allowing large models to be executed on a compute

cluster.

Another important aspect of creating models of GPR antennas is the ability to visualise, in 3D, their detailed geometrical features. Modelling these features required setting the properties of faces and edges of Yee cells in a finely discretised FDTD grid. ParaView (http://www.paraview.org/) is an open-source data-analysis and visualisation application based on the Visualisation Toolkit (VTK) (http://www.vtk.org/) and has been developed for handling extremely large datasets. The VTK is an open-source system for 3D computer graphics, image processing and visualisation. The VTK uses Extensible Markup Language (XML) files to define structured or unstructured grids that can contain data associated with each cell or cell vertex. A software toolset was developed using GprMax3D, the VTK, and Paraview that enabled the visualisation and manipulation of large finely discretised FDTD grids that could contain GPR antenna models.

Analysis of geometries and main components of the real antennas

Two widely-used antennas from leading GPR manufacturers — Geophysical Survey Systems, Inc. (GSSI) (http://www.ge and MALÅ Geoscience (http://www.malags.com/) — were studied. The GSSI 1.5 GHz (Model 5100) antenna and the MALÅ 1.2 GHz antenna are both high-frequency, high-resolution GPR antennas. These types of GPR antennas are primarily used for the evaluation of structural features in concrete: the location of rebar, conduits, and post-tensioned cables, as well as the estimation of material thickness on bridge decks and pavements.

The first, and arguably most important, stage in creating models of the antennas was to determine the geometry and materials of their main components. Some of these properties were readily obtained but others had to be determined using an optimisation process as they were both commercially sensitive and difficult to determine without specialist test equipment.

The geometry of the antennas and their components was the simplest information to input into the models. Both of the antennas are based on a configuration where the transmitter and receiver are in the same enclosure. Each enclosure was opened so that the main components could be studied, and these are highlighted in Figure 1(a) and Figure 1(b).

Both manufacturers use planar bowties for the transmitter (T_x) and receiver (R_x) elements of the antennas. The MALÅ 1.2 GHz antenna uses bowties with a flare angle of 85°, and resistive loading via discrete Surface Mount Technology (SMT) resistors. These resistors are attached at three locations on the open ends of the bowties, and are intended to reduce unwanted resonance at the expense of a reduction in radiation efficiency. The GSSI 1.5 GHz antenna uses bowties with a flare angle of 76° and additional rectangular patches added to the open ends of the bowtie. These extensions perform like straight sections of waveguide, which introduce a delay in the signal path and create destructive interference patterns that reduce unwanted resonance. In both antennas the bowties are etched from copper onto the Printed Circuit Boards (PCB). The bowties are enclosed in rectangular metal boxes which shield the antennas and also form part of the case for the MALÅ 1.2 GHz antenna.

Both antennas utilise an open-cell carbon-loaded foam which acts as a broadband electromagnetic absorber to reduce unwanted resonance in the cavities behind the bowties. These absorbers are similar to off-the-shelf broadband microwave absorbers, but are custom-made to manufacturers specifications which are commercially sensitive. Generally, carbon-loaded broadband microwave absorbers, e.g. Emerson and Cuming ECCOSORB® LS (http://www.eccosorb.com have a permeability of 1 but can have permittivities ranging from 1.25–30. As a consequence, the exact permittivity and conductivity values of the absorbers were unknown.

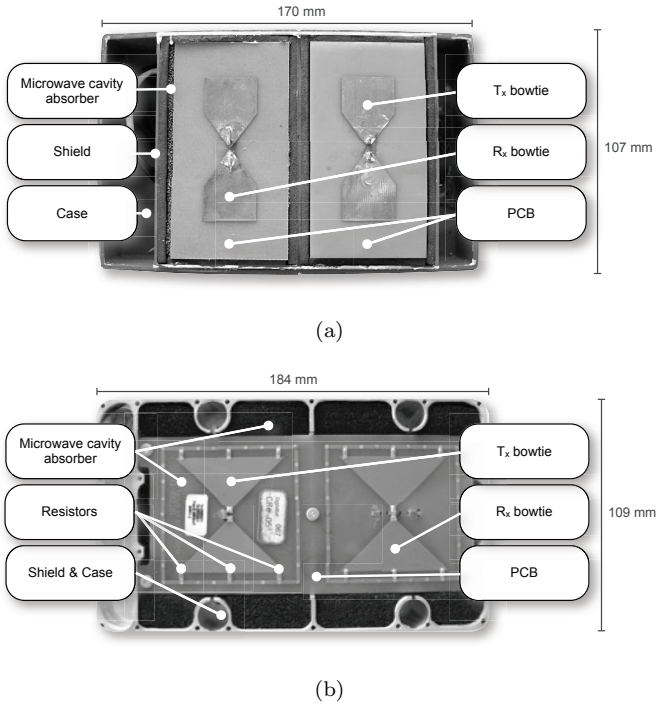

Figure 1: Annotated photographs of a) GSSI 1.5 GHz antenna, and b) MALÅ 1.2 GHz antenna with opened enclosures showing main components

The excitation of the antenna — pulse shape, frequency content, and feed method — is important for the performance of the real antenna, and hence critical to capture in the model. The shape and frequency content of the transmitted pulses used by GSSI and MALÅ were unknown and no specialist test equipment was available to measure them. In common with many other GPR simulations (Gurel and Oguz, 2000; Lee et al., 2004; Nishioka et al., 1999; Roberts and Daniels, 1997) a Gaussian shaped pulse was assumed with a centre frequency close to the manufac-

turers specification. Although a simple Gaussian shape is a good approximation, it may not be an entirely realistic representation of the real pulse shape. An investigation of different pulse shapes is planned for future development of the antenna models.

The transmitter and receiver bowties in the real antennas are connected to circuits that generate the transmitted pulse and process the received signals, respectively. There were two main reasons for not modelling the physical electronic components in these circuits:

- The circuit design, components, and component values were unknown and no specialist test equipment was available to measure them.
- To accurately model components of this size would have required a sub-millimetre FDTD mesh, which would have greatly increased the computational requirements.

Therefore a simplified feed model consisting of a voltage source with internal resistance inserted in a one-cell gap between the two arms of the transmitter bowtie (the drive-point) was used. The receiver circuitry was modelled as a lumped resistance using a cell edge with specific conductance inserted in a one-cell gap between the two arms of the receiver bowtie. The SMT resistors in the MALÅ antenna were modelled by distributing their known resistance over cell edges with specific conductance between the open ends of the bowties and the shield (ground plane).

FDTD model properties

GprMax3D input files for the antenna models were created from the analyses of the geometries and main components of the real antennas. Table 1 lists the electrical properties for the known materials, i.e. the metals and plastics which have well defined values for permittivity and conductivity. All metallic components in the antennas, apart from the copper bowties, were modelled as Perfect Electric Conductors (PEC).

Component	Material	ϵ_r	σ (S/m)
Bowtie	Copper	1.00	59.6×10^6
Skid plate	HDPE	2.35	0
PCB	Glass fibre	3.00	0
GSSI case	Polypropylene	2.26	0

Table 1: `Permittivity and conductivity values for the known materials used in the antennas`

Values for the following parameters were unknown:

- The centre frequency of the source pulse, f
- The resistance at the transmitter drive-point, R_{T_x}
- The resistance at the receiver, R_{R_x}
- The permittivity of the electromagnetic absorber, ϵ_r
- The conductivity of the electromagnetic absorber, σ

Figure 2(a) and Figure 2(b) show the FDTD meshes of the modelled geometries of the antennas. A spatial discretisation of $\Delta x = \Delta y = \Delta z = 1$ mm was chosen as a good compromise between accuracy and computational requirements. GprMax computes the spatial and temporal derivatives using a standard second-order scheme and this choice of spatial discretisation also ensured that any numerical dispersion was adequately controlled. The Courant Friedrichs Lewy (CFL) condition was enforced which resulted in a time-step of $\Delta t = 1.926$ ps.

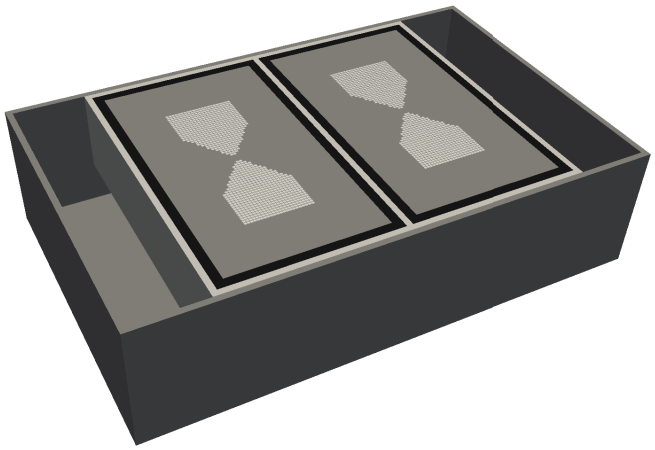

(a)

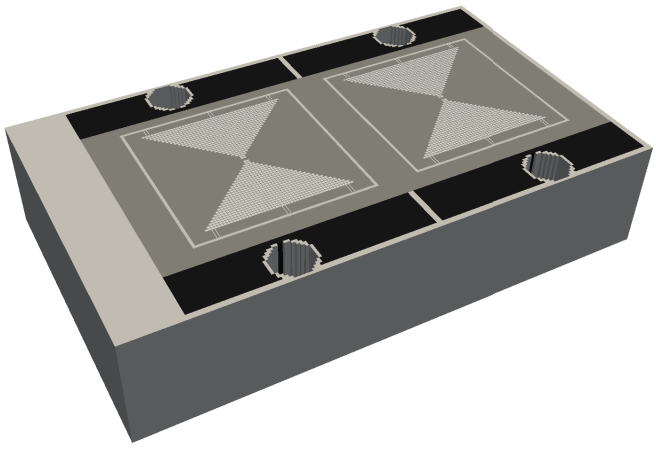

(b)

Figure 2: `FDTD meshes of modelled geometries of a) GSSI 1.5 GHz antenna, and b) MALÅ 1.2 GHz antenna`

OPTIMISATION OF THE MODELS

Several different optimisation methods, such as Artificial Neural Networks and Genetic Algorithms, were considered to establish values for the unknown parameters in the models. However, Taguchi's optimisation method was chosen for the following reasons:

- Simple to implement
- Effective in reduction of experiments
- Fast convergence speed
- Global optimum results
- Independence from initial values of optimisation parameters

Taguchi's method is based on the concept of the Orthogonal Array (OA) which can effectively reduce the number of experiments required in a design process (Taguchi et al., 2005). OAs provide a systematic method to determine parameter values so that an optimal result can be found from the fewest experiments. The notation $OA(N, k, s, t)$ is used to describe an OA. A formal description can be found in Hedayat et al. (1999), however, the mechanics of the OA can be understood by examining the simple example of an $OA(4, 3, 2, 2)$ shown in Table 2.

Experiments	Parameters		
	1	2	3
1	*0*	*0*	*0*
2	*0*	*1*	*1*
3	*1*	*0*	*1*
4	*1*	*1*	*0*

Table 2: `Structure of an` $OA(4, 3, 2, 2)$

There are 3 columns ($k = 3$) which means up to *3 different parameters* maybe studied, and there are 4 rows ($N = 4$) which means *4 different experiments* involving the parameters will be conducted. Since only 0's and 1's appear, this called a *2-level array* ($s = 2$). The levels can correspond to different parameter states, e.g. 'catalyst' or 'no catalyst', 'fast cooling' or 'slow cooling' etc., or numeric values depending on the application. The final part of the definition of the OA is the strength, and in this case the *strength is 2* ($t = 2$). This is the minimum number of columns needed to ensure that all the possible combinations of levels will occur. This is demonstrated in (1) where it is shown that 2 columns of the OA are necessary for all possible combinations of the levels to occur.

$$\textit{0}\quad \textit{0}, \qquad \textit{0}\quad \textit{1}, \qquad \textit{1}\quad \textit{0}, \qquad \textit{1}\quad \textit{1} \tag{1}$$

This ensures a balanced and fair comparison of levels for any parameter and any interactions of parameters. The strength of the OA should be large, but typically this is set at 2, 3 or 4 for real-world applications.

Obviously, even with a moderate number of parameters, and a small number of levels for each parameter, the number of possible combinations increases rapidly. It is, therefore, not always possible to make even one observation at each potential level combination. The purpose of the OA is to select which level combinations will be used, and these are known as fractional factorial experiments.

Since the rows of an OA represent experiments — which can require, money, time, and other resources — practical constraints require minimising the number of rows used. In addition, it is necessary to know the largest number of columns that can be used in the OA as this governs how many parameters can be studied.

A useful property of an OA is that any $N \times k'$ sub-array of an existing $OA(N, k, s, t)$ is still an OA with a notation of $OA(N, k', s, t')$, where $t' = \min\{k', t\}$. In other words, if one or more columns are deleted from the OA the result is still an OA but with a smaller number of parameters.

The method of construction of OAs is outside the scope of this paper, and is comprehensively dealt with by Hedayat et al. (1999). Many OAs with different parameters, levels, and strengths have been developed and archived in OA databases and libraries. The OAs used in this research were taken from the online library (http://www.research.att.com/~nj

Taguchi's optimisation method was implemented using the process shown in Figure 3.

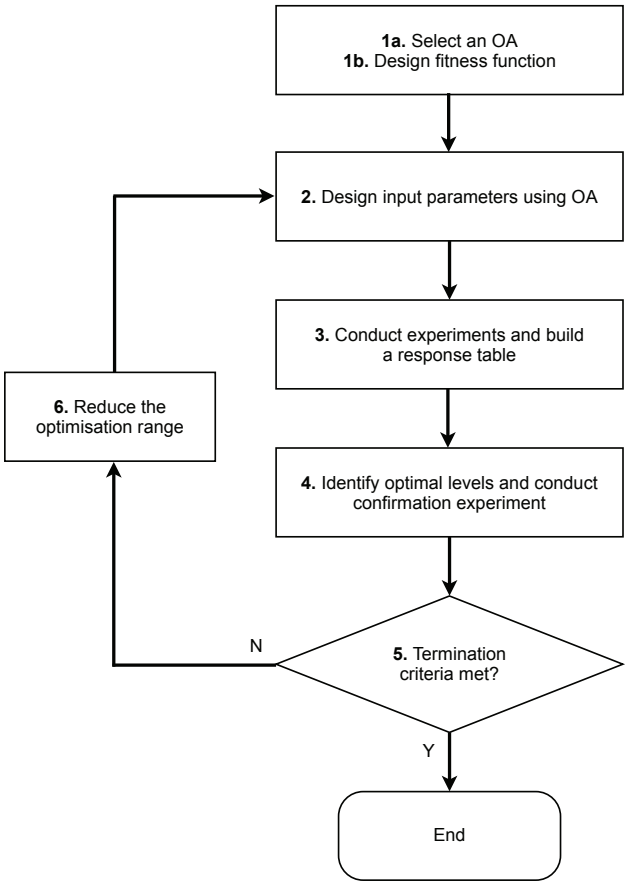

Figure 3: `Process of implementing Taguchi's method (Weng et al., 2007a,b)`

An important part of the Taguchi optimisation process was to develop a fitness function to assess the goodness of fit between the real and modelled responses of the an-

tennas. Therefore a characteristic response that could be obtained from both the real and modelled antennas was required. A parameter that could be easily measured from the real antennas was the crosstalk response in free-space. This was obtained by placing the antenna in free-space and recording the signal directly transmitted between the transmitter and receiver. A crosstalk response in free-space is an important parameter to characterise the performance and behaviour of an antenna, despite free-space not being representative of materials encountered in typical GPR surveys. Ideally, the response of a real antenna should be measured over a homogeneous material with a known permittivity close to that encountered in typical GPR surveys, however, this presents practical difficulties.

The computational domain of the antenna models was kept to a minimum for modelling the crosstalk response i.e. by using a well-performing PML the model domain only contained the antenna surrounded by a few cells of free-space. The domain for the GSSI 1.5 GHz antenna model was 270 × 207 × 143, and for the MALÅ 1.2 GHz antenna 284 × 209 × 140, resulting in approximately 8 million cells in each model. This required 600 MB of RAM and 30 minutes run-time on 6 CPU cores for a time window of 8 ns.

Figure 4(a) and Figure 4(b) show the results of the Taguchi optimisation process for the GSSI 1.5 GHz antenna, and the MALÅ 1.2 GHz antenna[†]. Both sets of results represent a 98% cross-correlation between the real and modelled crosstalk responses in free-space, achieved after 20 iterations of the Taguchi optimisation process. There are some small differences between the real and modelled responses evident: in the amplitudes of the initial part of the response, and the phase of the tail of the response for the GSSI 1.5 GHz antenna; and in the amplitudes of the response for the MALÅ 1.2 GHz antenna. The absorbers are designed to control resonance in cavities of the antennas, so it is possible that differences in the tail of the responses could be attributed to the properties of the absorbers not entirely captured in the models.

Table 3 lists the initial ranges that were specified for the unknown parameters as well as the converged values obtained as a result of the Taguchi optimisation process. Some of the converged values are realistic, e.g. the centre frequencies, and others are less so, e.g. the GSSI absorber permittivity. However, when all of these values are used in the antenna models very good matches for the real crosstalk responses in free-space can be achieved.

VALIDATION OF MODELS USING EMULSIONS

A series of laboratory experiments was conducted that used emulsions to replicate the electrical properties of real materials. Smith and Scott (1990) investigated emulsion

[†]The modelled crosstalk responses are the electric field values at the receiver antennas converted to voltages. Both modelled and real responses have been normalised to an absolute maximum amplitude of one, and have been corrected for any DC bias present.

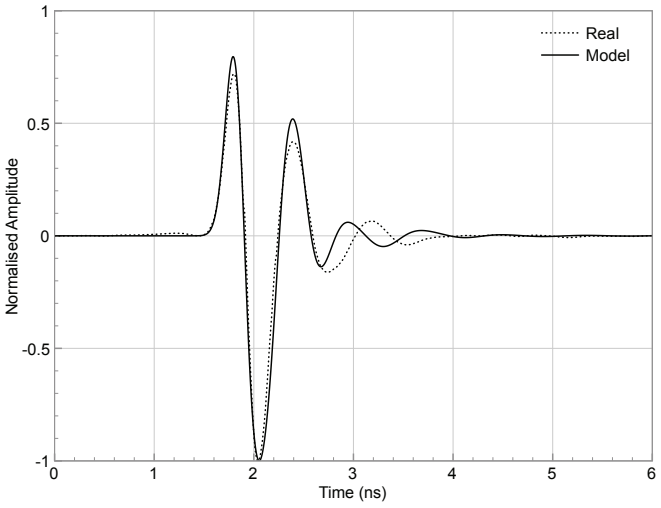

(a)

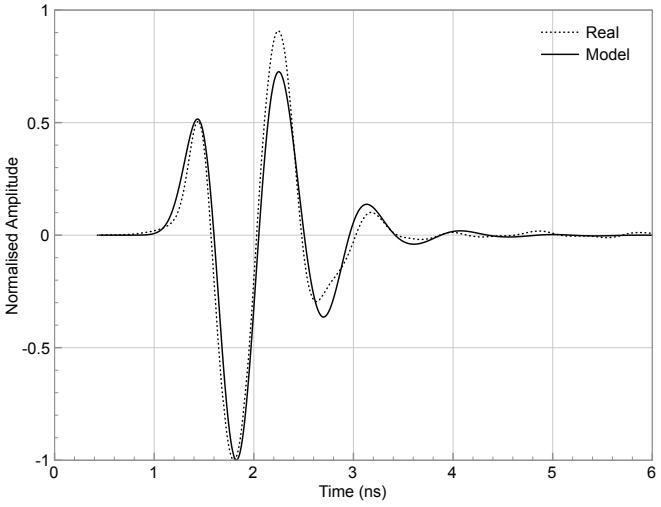

(b)

Figure 4: `Crosstalk responses in free-space from the optimised antenna models and the real antennas for a) GSSI 1.5 GHz antenna, and b) MALÅ 1.2 GHz antenna`

Parameter	Initial range	Converged value	
		GSSI	MALÅ
f (GHz)	0.8–2.5	1.71	0.978
Absorber ϵ_r	1–81	1.58	6.49
Absorber σ (S/m)	0.05–1	0.428	0.252
R_{T_x} (Ω)	0–1000	4	1000
R_{R_x} (Ω)	0–1000	925	891

Table 3: `Initial ranges and converged values for unknown parameters in the antenna models`

chemistry for the purposes of using emulsions in scale models of real GPR surveys. Bungey et al. (1993) and Infrasensec, Inc. (2003) also used emulsions to represent concrete slabs, and more recently Buff (2006) used gelatin to create a transparent substance with similar electrical properties to a variety of soils, loams and sands. The two main advantages of using emulsions are: they are homogeneous liquids with known and adjustable permittivity and conductivity values which can be definitively input into the simulations; and they enable a series of different targets to be easily embedded and tested.

The design and manufacture of the oil-in-water (O/W) emulsions was based on research by Smith and Scott (1990) . The *mineral oil* (disperse phase) was assumed to be a lossless dielectric with a constant real relative permittivity independent of frequency and temperature,

$$\epsilon_{r1} = 2.27, \tag{2}$$

and with negligible conductivity,

$$\sigma_1 = 0 \tag{3}$$

The *saline solution* (continuous phase) has a complex permittivity described by the Debye equation,

$$\epsilon_r(T, N) = \epsilon_{r\infty} + \frac{\epsilon_{r0}(T, N) - \epsilon_{r\infty}}{1 + j\omega\tau(T, N)}, \tag{4}$$

and a real frequency independent conductivity,

$$\sigma = \sigma_2(T, N) \tag{5}$$

It has been shown that dispersion in the electrical properties of O/W emulsions can be described in a straightforward manner. For frequencies less than 3 GHz, the relative permittivity is approximately constant and equal to a low-frequency value,

$$\bar{\epsilon}_r \approx \bar{\epsilon}_{rLF} \tag{6}$$

where,

$$\bar{\epsilon}_{rLF}(T, N, \Phi_1) = \frac{1}{2}\left(3\epsilon_{r1} + (1 - \Phi_1)^{\frac{3}{2}}\left(2\epsilon_{r0}(T, N) - 3\epsilon_{r1},\right)\right) \tag{7}$$

which is dependent upon the temperature and normality of the saline solution, and the volume fraction of the mineral oil, Φ_1. The conductivity of the emulsions is given by a constant low-frequency value plus a term which increases with the square of the frequency.

$$\tilde{\bar{\sigma}} = \bar{\sigma}_{LF} + \Delta\tilde{\bar{\sigma}} \tag{8}$$

where,

$$\bar{\sigma}_{LF}(T, N, \Phi_1) = \sigma_2(T, N)\,(1 - \Phi_1)^{\frac{3}{2}} \tag{9}$$

and,

$$\Delta\tilde{\bar{\sigma}} = \frac{\epsilon_{rLF}\,(2\epsilon_{r0} + \epsilon_{r1})\,(\bar{\epsilon}_{rLF} - \epsilon_{r1})}{\epsilon_{r0}\,(2\bar{\epsilon}_{rLF} + \epsilon_{r1})\,(\epsilon_{r0} - \epsilon_{r1})}\epsilon_0\,(\epsilon_{r0} - \epsilon_{r\infty})\,\tau\omega^2 \tag{10}$$

Numerical values for the average electrical constitutive parameters $\bar{\epsilon}_r$ and $\tilde{\bar{\sigma}}$ of the emulsions can be calculated from specified ϵ_{r1}, Φ_1, the normality of the saline solution N, and temperature T, and using equations (7) and (8). The relative permittivity $\bar{\epsilon}_{rLF}$ is seen to depend mainly on the volume fraction of oil Φ_1, while the conductivity $\bar{\sigma}_{LF}$ depends mainly on the normality of the saline solution N. Both $\epsilon_{r\bar{L}F}$ and $\tilde{\bar{\sigma}}$ are adjustable over wide ranges: $10 \leq \bar{\epsilon}_{rLF} \leq 80$ and 4×10^{-4} S/m $\leq \tilde{\bar{\sigma}} \leq 4$ S/m.

It was decided to make three emulsions with permittivities around 10, 20 and 30 spanning a wide range of common materials encountered in GPR surveys. The chemicals used to make the emulsions were: Millube 32 – a non-additive lubricating oil[‡]; emulsifiers – Tween® 20 (polyoxyethylene sorbitan monolaurate) and Span® 80 (sorbitan monooleate)[§]; and distilled water. The basic apparatus used for the experiments consisted of: a 50 L galvanised steel tank, a perspex rig to mount each antenna and corresponding Distance Measurement Instrument (DMI), a high-shear batch mixer, and a 25 L plastic mixing vessel. Figure 5 shows the tank apparatus with the antenna holder and attached GSSI DMI, which could be slid from one end of the tank to the other, allowing B-scans to be recorded.

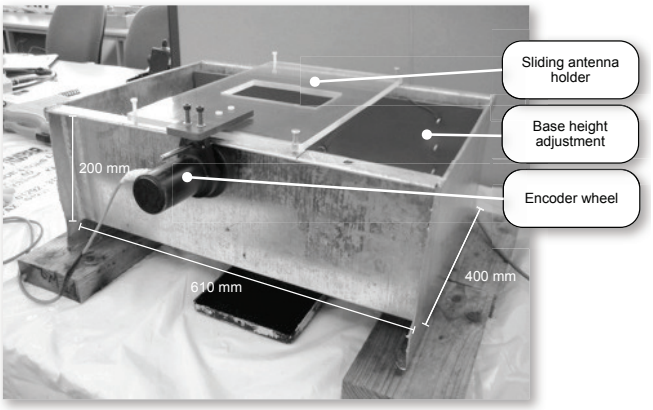

Figure 5: `Annotated photograph of tank rig used for laboratory experiments`

As an approximate check of the permittivities of the emulsions, mineral oil and the distilled water, some simple time difference measurements were made. For each liquid, an A-scan was recorded with the antenna in the centre of the tank and the tank base at its lowest height. The depth of the liquid was measured at this base position. The base was then raised 50 mm and another A-scan recorded. Figure 6 shows an example of the two measurements with the time difference Δt, between corresponding points in the reflection wavelet from the base, highlighted. The distance travelled was calculated using

[‡]Millube is a trademark of Millers Oils, Ltd.
[§]Tween® and Span® are trademarks of ICI Americas, Inc.

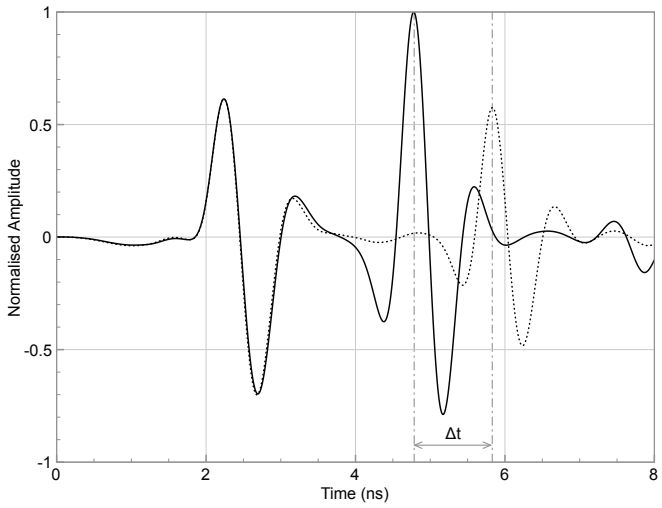

Figure 6: Example A-scans of reflections from tank base at two different base heights

the known depth of the liquid and the separation of the transmitter and receiver elements in the antenna. This was used along with the time difference Δt to calculate the velocity, and subsequently the relative permittivity of each liquid. Table 4 lists the theoretical and measured permittivities for all the liquids, which agree well. The average measured values were used in the models.

	Theoretical ϵ_r	Measured ϵ_r
Mineral oil	2.27	2.19 ± 0.07
Emulsion 1	10.17	10.34 ± 0.20
Emulsion 2	19.74	19.00 ± 0.30
Emulsion 3	30.15	32.03 ± 0.53
Distilled water	79.12	78.74 ± 1.13

Table 4: Theoretical and measured permittivities for the emulsions and their constituents ($T = 23°C$)

The following targets, typically investigated using GPR, were tested with the emulsions:

- 8 mm, 10 mm, and 12 mm diameter steel rebar
- 8 mm diameter Carbon Fibre Reinforced Polymer (CFRP) rebar
- 9 and 32 mm diameter Glass Fibre Reinforced Polymer (GFRP) rebar
- 120×95×55 mm metal box

All of the targets were tested with both GPR systems in all of the liquids[¶]. A-scans were taken by placing the antenna directly over the target which was on the centreline of the tank, and recording data for a fixed period of time. B-scans were taken by moving the antenna from one end of the tank to the other with a DMI attached. In all tests the antennas were submerged in the liquid to the top of their skid plates ensuring no air gap existed.

Modelling the experimental setup

Numerical models of the experimental setups were created in GprMax3D, and included the GSSI or MALÅ antenna model, the steel tank filled with one of the liquids, and one of the different target configurations. One of the most important aspects of simulating the experiments was accurately model the electrical properties of the liquids. The mineral oil had a constant permittivity and negligible conductivity. The losses in the distilled water were modelled using the standard Debye equation. The permittivities of the emulsions were constant over the bandwidth of interest for GPR. The conductivities of the emulsions were described by a constant low frequency value of conductivity σ_{LF}^{-} plus a term $\Delta\tilde{\sigma}$ which increased as the square of frequency (8). Initially it was attempted to model this dispersive conductivity using a simple DC value. Figure 7 clearly shows that the amplitudes of the responses from models with DC conductivity do not match the real responses. A better method for modelling the real dispersive conductivity was required. Similar to the work of Bourgeois and Smith (1996) a single term Debye model was used with modified $\epsilon_{r\infty}$ and τ parameters, listed in Table 5. Figure 8 shows the fitted Debye models match the real dispersive conductivity behaviour of the emulsions, and result in the *Debye fit* response of Figure 7.

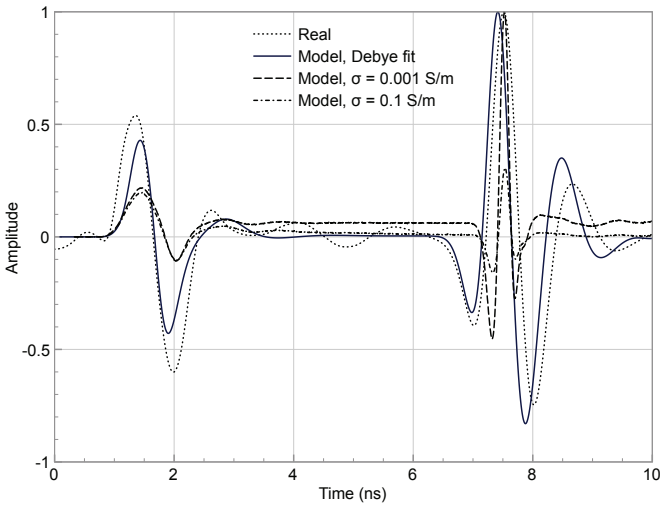

Figure 7: GSSI 1.5 GHz antenna: Modelled vs. real A-scans with different values of DC conductivity, no target in tank, and emulsion, $\epsilon_r = 32.03$

[¶]Temperature T was measured at 23°C.

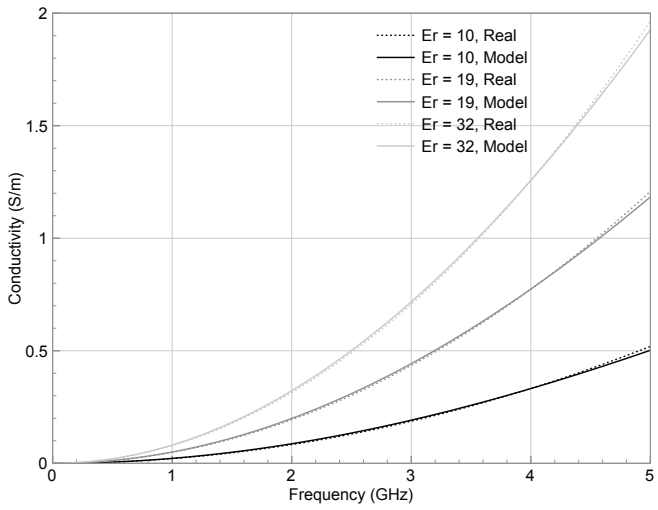

Figure 8: Dispersive conductivity of the emulsions over bandwidth of interest for GPR

	ϵ_{r0}	$\epsilon_{r\infty}$	$\tau(s)$
Emulsion 1	10.34	4.0	9.95×10^{-12}
Emulsion 2	19.00	1.0	8.00×10^{-12}
Emulsion 3	32.03	1.0	7.50×10^{-12}

Table 5: Modified parameters used in the Debye model for the dispersive conductivities of the emulsions

Comparison of experimental and modelled responses

One target configuration (12 mm steel rebar) and one antenna (GSSI 1.5 GHz) have been chosen to compare the real and modelled responses in all of the liquids. Analyses of responses from the MALÅ 1.2 GHz antenna yielded similar results to those of the GSSI 1.5 GHz model.

Figures 9–13 show the real versus modelled responses in ascending order of permittivities of the liquids. All the responses have been aligned by their first break.

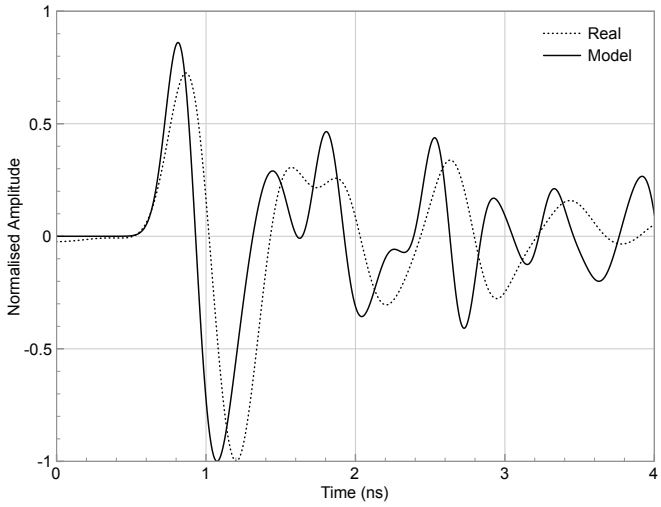

Figure 9: GSSI 1.5 GHz antenna: Modelled vs. real A-scans of a 12 mm steel rebar in mineral oil, $\epsilon_r = 2.27$

Figure 9 shows the real and modelled responses in mineral oil. The mineral oil has a low permittivity ($\epsilon_r = 2.27$) and therefore high velocity, which combined with the proximity of the target to the antenna means that wavelets from the rebar and the base of the tank overlap one another as well as the direct wave. It is precisely this type of response that demonstrates the need to have an accurate antenna model in the simulation. The direct wave in the real response is fairly well predicted by the model, minor differences being a slightly larger first positive peak and slightly narrower waveshape in the modelled response. The wavelets from metallic targets (the rebar and base of the tank) are difficult to separately distinguish. The modelled response contains additional ripples in the tail of the signal that are not present in the real response.

Figure 10 shows the real and modelled responses in the first of the emulsions, $\epsilon_r = 10.34$. The wavelets in the responses that correspond to the direct wave, rebar, and base of tank have been annotated to aid interpretation in this, and further figures. Again, the direct wave is well predicted by the model, exhibiting a similar set of minor differences to the mineral oil. Due to the increased permittivity, the wavelet from the rebar is almost separable from the direct wave and along with the wavelet from the

base of the tank can now be easily identified. The arrival times and shapes of these wavelets are fairly well predicted by the model with minor overshoots in amplitude.

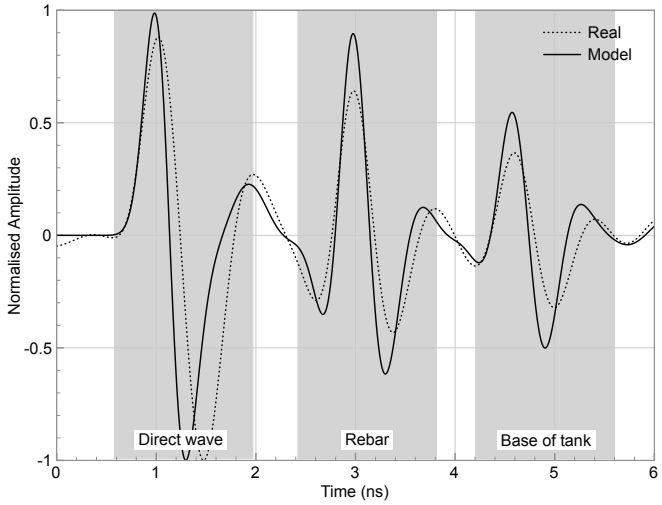

Figure 10: `GSSI 1.5 GHz antenna: Modelled vs. real A-scans of a 12 mm steel rebar in emulsion,` $\epsilon_r = 10.34$

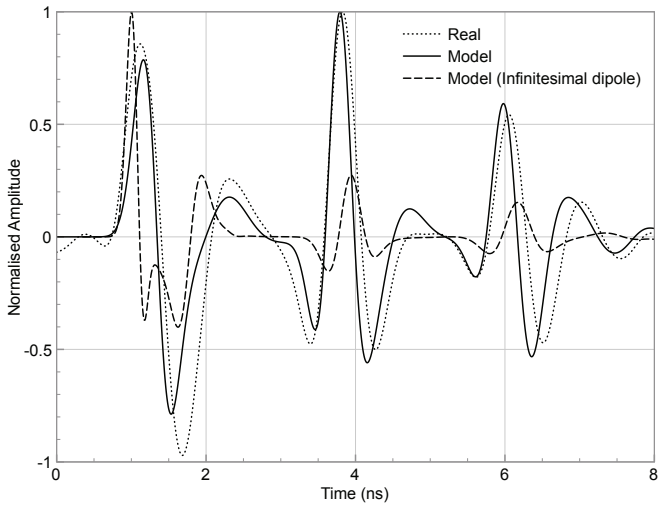

Figure 11: `GSSI 1.5 GHz antenna: Modelled vs. real A-scans of a 12 mm steel rebar in emulsion,` $\epsilon_r = 19.00$

Figure 11 shows the real and modelled responses in the emulsion, $\epsilon_r = 19.00$. The model behaviour is very similar to the previous emulsion but with an even better match for the amplitudes of the wavelets from the rebar and the base of the tank. Figure 11 also contains a response from an identical simulation where the antenna was completely replaced by a theoretical source model—an infinitesimal dipole. This clearly highlights the differences between using a realistic description of an antenna and using a theoretical source model. It can be seen that although there is

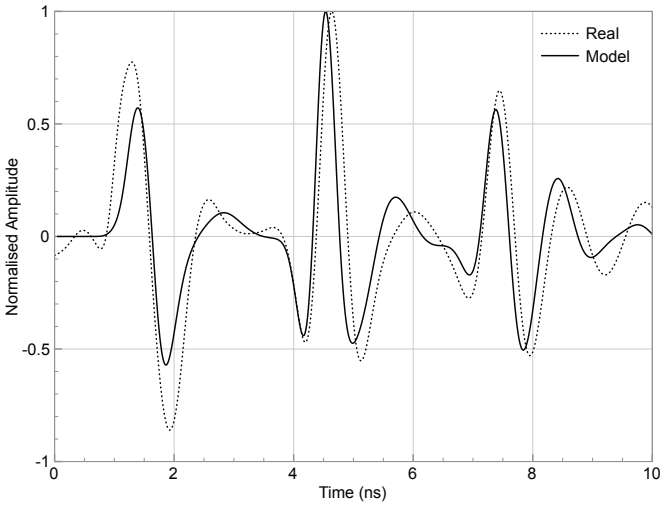

Figure 12: `GSSI 1.5 GHz antenna: Modelled vs. real A-scans of a 12 mm steel rebar in emulsion,` $\epsilon_r = 32.03$

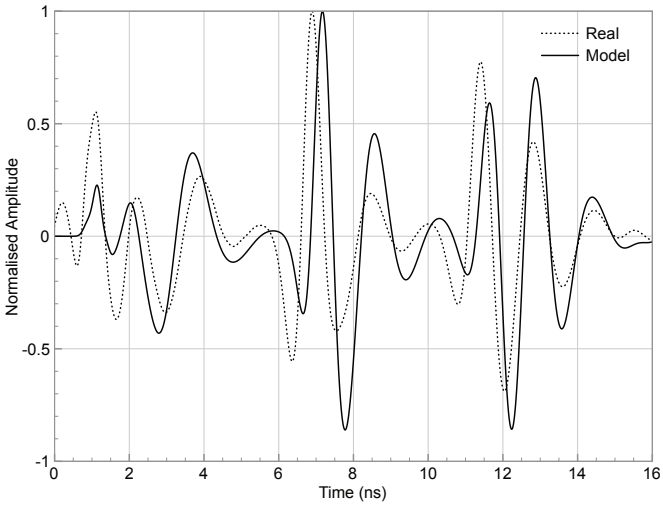

Figure 13: `GSSI 1.5 GHz antenna: Modelled vs. real A-scans of a 12 mm steel rebar in distilled water,` $\epsilon_r = 78.90$

similarity in the shapes of the wavelets, the arrival times are not that well predicted, and amplitude information is not reproduced in the theoretical source model.

Figure 12 shows the real and modelled responses in the last of the emulsions, $\epsilon_r = 32.03$, and Figure 13 shows the real and modelled responses in the distilled water, $\epsilon_r = 78.90$. As the permittivity of the liquid increases, it can be observed that the model under-predicts the amplitude of the direct wave, and in the case of the distilled water, does not well-predict the shape. This is likely attributed to fact that the unknown parameters in the antenna models were optimised using the crosstalk response in free-space of the real antennas. As such, it can be concluded that the coupling effects between the antenna and the liquid are better optimised for lower permittivities. Despite the discrepancies in the modelled direct waves, the modelled responses from the rebar and base of the tank show very good agreement with the real data.

The general performance and accuracy of the models can also be assessed by comparing B-scans of typical GPR targets. Figure 14(a) shows the real B-scan, and Figure 14(b) the modelled B-scan of a 12 mm steel rebar in the emulsion, $\epsilon_r = 32.03$. The cylindrical shape of the rebar yields a typical hyperbolic response, and the response from the base of the tank is clearly evident at approximately 7 ns. Under the centre of the hyperbola the response from the base of the tank has reduced amplitude caused by masking from the steel rebar. Reflections from the corners of tank which appear as partial hyperbolas can be seen at either side of the B-scan from approximately 8.5–12 ns. All of these features which are present in the real data are well predicted by the model.

CONCLUSIONS

To accurately predict the phase and amplitude of GPR responses for near-surface, near-field targets it is essential that a GPR forward model contains a realistic description of the antennas. Detailed 3D FDTD models of two commercial high-frequency GPR antennas—a GSSI 1.5 GHz antenna and a MALÅ 1.2 GHz antenna—have been developed from simple analyses of the geometries and main components of the antennas. Taguchi's optimisation method was successfully used to determine values of unknown parameters in the antennas. The result of the optimisation was a 98% cross-correlation match of the modelled and real crosstalk responses in free-space for both antennas.

Further validation was carried out using a series of oil-in-water emulsions to simulate the electrical properties of real materials. A range of steel and composite rebar and a rectangular metallic box were embedded in the emulsions as targets. We have found that it is critical to correctly model both the permittivity and dispersive conductivity behaviour of the emulsions, without which it is not possible to accurately predict both phase and amplitude information. A-scan and B-scans of a 12 mm steel rebar in the different emulsions with the GSSI 1.5 GHz antenna

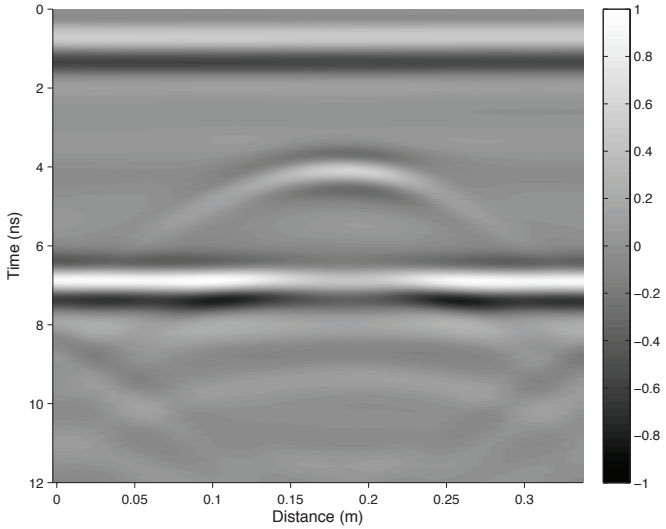

(a)

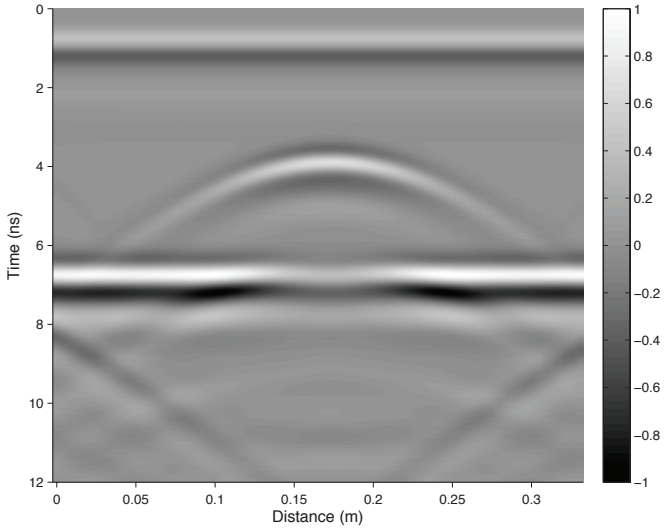

(b)

Figure 14: GSSI 1.5 GHz antenna: (a) Real, (b) Modelled B-scans of a 12 mm steel rebar in emulsion, $\epsilon_r = 32.03$

showed that the modelled responses were in good agreement with the real data in terms of the amplitude, phase and shape of the different wavelets. Small differences between the real and modelled responses were more apparent in the higher permittivity liquids. This was attributed to the values of the unknown parameters in the antennas being optimised for free-space. The accuracy of both the GSSI 1.5 GHz antenna and MALÅ 1.2 GHz antenna models was generally very good and this provides confidence for their use in more advanced studies.

ACKNOWLEDGEMENTS

The authors would like to acknowledge the reviewers of this paper, Tim Bergmann, Sébastien Lambot and Charles Oden, for their helpful comments and suggestions.

REFERENCES

Berenger, J., 1994, A perfectly matched layer for the absorption of electromagnetic waves: Journal of Computational Physics.

Bourgeois, J., and G. Smith, 1996, A fully three-dimensional simulation of a ground-penetrating radar: Fdtd theory compared with experiment: IEEE Transactions on Geoscience and Remote Sensing, **34**, 36–44.

Buff, P. M., 2006, Characterization of propagation on wires over lossy earth: PhD thesis, North Carolina State University.

Bungey, J., S. Millard, and M. Shaw, 1993, Simulation tank to aid interpretation of radar results on concrete: Magazine of Concrete Research, **45**, 187–195.

Galagedara, L., J. Redman, G. Parkin, A. Annan, and A. Endres, 2005, Numerical modeling of GPR to determine the direct ground wave sampling depth: Vadose Zone Journal, **4**, 1096–1106.

Gedney, S., 1996, An anisotropic PML absorbing media for the FDTD simulation of fields in lossy and dispersive media: Electromagnetics, **16**, 399–415.

Giannopoulos, A., 2005, Modelling ground penetrating radar by gprmax: Construction and Building Materials, 755–762.

Gurel, L., and U. Oguz, 2000, Three-dimensional FDTD modeling of a ground-penetrating radar: IEEE Transactions on Geoscience and Remote Sensing, **38**, 1513–1521.

Hedayat, A., N. Sloane, and J. Stufken, 1999, Orthogonal arrays: Theory and applications: Springer-Verlag.

Holliger, K., B. Lampe, U. Meier, M. Lambert, and A. Green, 2003, Realistic modeling of surface ground-penetrating radar antenna systems: where do we stand?: Proceedings of the 2nd International Workshop on Advanced Ground Penetrating Radar, 45–50.

Huang, Z., K. Demarest, and R. Plumb, 1999, An FDTD/MoM hybrid technique for modeling complex antennas in thepresence of heterogeneous grounds: IEEE Transactions on Geoscience and Remote Sensing, **37**, 2692–2698.

Infrasensec, Inc., 2003, Non-destructive measurement of pavement layer thickness: Technical report, California Department of Transportation.

Jeannin, M., S. Garambois, C. Grégoire, and D. Jongmans, 2006, Multiconfiguration GPR measurements for geometric fracture characterization in limestone cliffs (Alps): Geophysics, **71**, B85.

Klysz, G., X. Ferrieres, J. Balayssac, and S. Laurens, 2006, Simulation of direct wave propagation by numerical fdtd for a gpr coupled antenna: NDT and E International, **39**, 338–347.

Lambot, S., F. Andre, K. Jadoon, E. Slob, and H. Vereecken, 2010, Full-waveform modeling of ground-coupled gpr antennas for wave propagation in multi-layered media: the problem solved?: 13th International Conference on Ground Penetrating Radar, 898—902.

Lambot, S., E. Slob, and I. van den Bosch, 2004, Modeling of ground-penetrating radar for accurate characterization of subsurface electric properties: IEEE Transactions on Geoscience and Remote Sensing, **42**, 2555–2567.

Lee, K.-H., C.-C. Chen, F. Teixeira, and R. Lee, 2004, Modeling and investigation of a geometrically complex uwb gpr antenna using fdtd: IEEE Transactions on Antennas and Propagation, **52**, 1983–1991.

Lestari, A., A. Yarovoy, and L. Ligthart, 2004, RC-loaded bow-tie antenna for improved pulse radiation: IEEE Transactions on Antennas and Propagation, **52**, 2555–2563.

———, 2005, Adaptive wire bow-tie antenna for GPR applications: IEEE Transactions on Antennas and Propagation, **53**, 1745–1754.

Liu, L., Y. Su, and J. Mao, 2008, FDTD analysis of ground-penetrating radar antennas with shields and absorbers: Frontiers of Electrical and Electronic Engineering in China, **3**, 90–95.

Lopera, O., and N. Milisavljevic, 2007, Prediction of the effects of soil and target properties on the antipersonnel landmine detection performance of ground-penetrating radar: A Colombian case study: Journal of Applied Geophysics, **63**, 13–23.

Monorchio, A., A. Bretones, R. Mittra, G. Manara, and R. Martin, 2004, A hybrid time-domain technique that combines the finite element, finite difference and method of moment techniques to solve complex electromagnetic problems: IEEE Transactions on Antennas and Propagation, **52**, 2666–2674.

Nishioka, Y., O. Maeshima, T. Uno, and S. Adachi, 1999, Fdtd analysis of resistor-loaded bow-tie antennas covered with ferrite-coated conducting cavity for subsurface radar: IEEE Transactions on Antennas and Propagation, **47**, 970–977.

Oden, C., 2006, Calibration and data processing techniques for ground penetrating radar systems with applications in dispersive ground: PhD thesis, Colorado School of Mines, Golden, CO.

Roberts, R. L., and J. J. Daniels, 1997, Modeling near-

field gpr in three dimensions using the fdtd method: Geophysics, **62**, 1114–1126.

Shlager, K., G. Smith, and J. Maloney, 1994, Optimization of bow-tie antennas for pulse radiation: IEEE Transactions on Antennas and Propagation, **42**, 975–982.

Smith, G., and W. Scott, 1990, The use of emulsions to represent dielectric materials in electromagnetic scale models: IEEE Transactions on Antennas and Propagation, **38**, 323–334.

Soldovieri, F., J. Hugenschmidt, R. Persico, and G. Leone, 2007, A linear inverse scattering algorithm for realistic GPR applications: Near Surface Geophysics, **5**, 29–42.

Streich, R., and J. van der Kruk, 2007, Characterizing a gpr antenna system by near-field electric field measurements: Geophysics.

Taguchi, G., S. Chowdbury, and Y. Wu, 2005, Taguchi's quality engineering handbook: John Wiley and Sons, Inc.

Uduwawala, D., and M. Norgren, 2006, An investigation of some geometrical shapes and selection of shielding and lumped resistors of planar dipole antennas for GPR applications using FDTD: IEEE Transactions on Geoscience and Remote Sensing, **44**, 3555–3562.

Uduwawala, D., M. Norgren, P. Fuks, and A. Gunawardena, 2004, A deep parametric study of resistor-loaded bow-tie antennas for ground-penetrating radar applications using fdtd: IEEE Transactions on Geoscience and Remote Sensing, **42**, 732–742.

———, 2005, A complete FDTD simulation of a real GPR antenna system operating above lossy and dispersive grounds: Progress In Electromagnetics Research, 209–229.

van Coevorden, C., A. Bretones, M. Pantoja, F. Ruiz, S. Garcia, and R. Martin, 2006, GA design of a thin-wire bow-tie antenna for GPR applications: IEEE Transactions on Geoscience and Remote Sensing, **44**, 1004–1010.

Weng, W.-C., F. Yang, and A. Z. Elsherbeni, 2007a, Electromagnetics and antenna optimization using taguchi's method: Morgan and Claypool Publishers.

———, 2007b, Linear antenna array synthesis using taguchi's method: A novel optimization technique in electromagnetics: IEEE Transactions on Antennas and Propagation, **55**, 723–730.

Wensink, W., G. Greeuw, J. Hofman, and J. Deen, 1990, Measured underwater near-field E-patterns of a pulsed, horizontal dipole antenna in air: Comparison with the theory of the continuous wave, infinitesimal electric dipole: Geophysical Prospecting, **38**, 805–830.

Wensink, W., J. Hofman, and J. Deen, 1991, Measured reflection strengths of underwater pipes irradiated by a pulsed horizontal dipole in air: Comparison with continuous plane-wave scattering theory: Geophysical Prospecting, **39**, 543–566.